Computing surface acidity constants of proton hopping groups from density functional theory based molecular dynamics: application to SnO2(110)/H2O interface

Mei Jia[1], Chao Zhang[2], Stephen J. Cox[3], Michiel Sprik[3], Jun Cheng[1*]

[1]College of Chemistry and Chemical Engineering, Xiamen University, Xiamen, Fujian 361005, P. R. China

[2]Department of Chemistry–Ångström Laboratory, Uppsala University, Lägerhyddsvägen 1, P. O. Box 538, 75121 Uppsala, Sweden

[3]Department of Chemistry, University of Cambridge, Cambridge CB2 1EW, United Kingdom

Proton transfer at metal oxide/water interfaces plays an important role in electrochemistry, geochemistry and environmental science. The key thermodynamic quantity to characterize this process is the surface acidity constant. An ab initio method that combines density functional theory based molecular dynamics (DFTMD) and free energy perturbation theory has been established for computing surface acidity constants. However, it involves a reversible proton insertion procedure in which frequent proton hopping, e.g. for strong bases and some oxide surfaces (e.g. SnO_2), can cause instability issues in electronic structure calculation. In the original implementation, harmonic restraining potentials are imposed on all O-H bonds (denoted by the V_{rH} scheme) to prevent proton hopping, and thus may not be applicable for systems involving spontaneous proton hopping. In this work, we introduce an improved restraining scheme with a repulsive potential V_{rep} to compute the surface acidities of systems in which proton hopping is spontaneous and fast. In this V_{rep} scheme, a Buckingham-type repulsive potential V_{rep} is applied between the deprotonation site and all other protons in DFTMD simulations. We first verify the V_{rep} scheme by calculating the pK_a's of H_2O and aqueous HS^- solution (i.e. strong conjugate bases), and then apply it to the $SnO_2(110)/H_2O$ interface. It is found that the V_{rep} scheme leads to a prediction of the point of zero charge (PZC) of 4.6, which agrees well with experiment. The intrinsic individual pK_a of terminal five-coordinated Sn site ($Sn_{5c}OH_2$) and bridge oxygen site ($Sn_2O_{br}H^+$) are 4.4 and 4.7, respectively, both being almost the same as the PZC. The similarity of the two pK_a values indicate that dissociation of terminal water has almost zero free energy at this proton hopping interface (i.e. partial water dissociation), as expected from the acid-base equilibrium on SnO_2.

---

* chengjun@xmu.edu.cn

1. Introduction

Since proton transfer (PT) is ubiquitous in chemical, biological and geochemical systems, lots of attention has been paid to PT processes both in experiment and theory[1-9]. Acidity constants (pK_a) are the key parameter measuring thermodynamic properties of PT processes in solution and at oxide/water interfaces. At metal oxide/water interfaces, there are many chemically active sites which can interact with water molecules, and exchange protons with bulk water or neighboring sites[10]. The change of protonation states of surface groups depends on their pK_a values and pH in solution. There is a special pH condition at which the oxide surface possesses no net proton charge, i.e. the point of zero proton charge (PZC). When the pH in solution is lower than the PZC, the oxide surface will accept protons from solution and become positively charged, and when the pH is above the PZC, the surface will release protons to solution and become negatively charged[11,12].

Although PZC can be measured by the potentiometric titration method, the intrinsic pK_a's of individual surface groups are generally inaccessible by experiment. Note that recent advances in wide-field second harmonic spectroscopy methods are making some headway in resolving this issue.[13-16] Theoretical calculations therefore offer an appealing alternative to determine surface acidities. Along these lines, previous theoretical approaches include the bond valence methods of Bickmore and co-workers,[11,17-19] and Hiemstra *et al*'s MUltiSIte Complex (MUSIC) model,[20] while Machesky and co-workers used classical molecular dynamics (MD) simulations and density functional theory (DFT) structural optimization to obtain bond valences and predict pK_a's.[21-23] Despite many successes, the accuracy of predicted individual pK_a's with these methods inherently depends on the empirical parameters used.

An alternative approach for predicting individual pK_a values, which avoids the need to introduce empirical parameters, is to combine all atom DFTMD and free energy perturbation (FEP) methods.[24-30] In this DFTMD approach, the free energy of proton transfer can be derived from the vertical energy gap between the protonated (HX) and deprotonated state (X$^-$) in a reversible proton insertion procedure.[24] In this procedure, the vertical energy gap is computed by switching off the proton's nuclear charge, turning it into a "dummy" atom. This dummy proton has no interactions with other atoms in the simulated models except that a harmonic restraining potential V_{rd} is applied to it to keep where the proton was. In the early implementation, to prevent instability an addition restraining potential V_{rH} was applied to all O-H bonds that may dissociate spontaneously, which has been used to good effect to calculate pK_a's of molecular acids, like benzoquinone[26], tyrosine and tryptophan[27], the mineral-water

interfaces like quartz and gibbsite[31-35] and the oxide-water interfaces like rutile TiO_2[36,37] and hematite (α-Fe_2O_3)[38]. In the systems mentioned above, proton hopping among surface groups is a rare event and DFTMD simulations[39-41] with the V_{rH} scheme can be safely performed. However, the applicability of this approach to systems where O-H groups release protons spontaneously, such as $RuO_2(110)$[42,43], $ZnO(100)$[44,45], cubic ZrO_2[46], $InP(001)$[47], β-$MnO_2(110)$[48] and $SnO_2(110)$ interface[22,49-52], remains a problem.

In this work, we introduce an improved restraining scheme to the DFTMD based method for computing the acidities in systems with proton hopping groups. In this modified scheme, a Buckingham-type repulsive potentials V_{rep} is applied between the deprotonation site X^- and all other protons in DFTMD simulations, instead of imposing a harmonic restraining potential V_{rH} to all O-H bonds. We first verify the V_{rep} scheme by calculating the pK_a's of H_2O and aqueous HS^- solution, and then apply it to the rutile $SnO_2(110)/H_2O$ interface. Our study shows that in contrast to the V_{rH} scheme, the proposed V_{rep} scheme leads to a consistent thermodynamic description of surface pK_a's, the point of zero charge (PZC) and water dissociation free energy ΔA_{diss} at oxide/liquid interfaces where surface water can spontaneously dissociate with frequent proton hopping events.

2. Theory and Methods

2.1. Calculation of pK_a's by free energy perturbation

An acid dissociation reaction can be written as,

$$XH \rightarrow X^- + H^+(aq) \qquad (1)$$

where X denote a molecular group or acid-base active site on a surface. The acid dissociation free energy of reaction (1) is $\Delta G_a^o = 2.3 k_B T p K_a$, where T is the temperature and k_B is the Boltzmann constant. DFTMD implementation of the free energy perturbation method has been developed for computing acid dissociation energies and pK_a's, in which free energy changes can be obtained by integrating ensemble averages of vertical energy gaps computed from a series of MD trajectories sampling configurations transforming from reactant to product state[24,26,27]. The method is briefly described as follows.

For the protonated reactant XH transforms into the deprotonated product X^-, we can construct a mapping potential energy function E_η, which is a linear superposition of the potential energy function of the protonated state E_{XH} and deprotonated state E_{X^-},

$$E_\eta = (1-\eta)E_{XH} + \eta E_{X^-} \quad (2)$$

where η is the coupling parameter varying from 0 (i.e. reactant XH) to 1 (i.e. product X^-). As described in previous publications[24,26-28,30,36], the transferred proton in reaction (1) is inserted or removed by switching off its nuclear charge and transforming it into a 'dummy' proton as a half reaction,

$$XH \rightarrow Xd^- \quad (3)$$
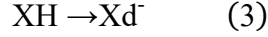
When combining Eq. (3) with $H_2Od \rightarrow H_3O^+$, it will make a full proton transfer reaction. As the dummy proton does not have interactions with other atoms in the simulated model, a harmonic restraining potential V_{rd} is applied between the dummy proton and X^- site both for XH state and Xd^- state in DFTMD simulations[24,53]. Including the contribution of V_{rd}, the restrained mapping potential expression is modified to read,

$$E_\eta = (1-\eta)E_{XH} + \eta E_{X^-} + V_{rd} \quad (4)$$

The introduced V_{rd} ensures that the dummy proton is kept its position close to the equilibrium position of the H^+ nucleus in the protonated state HX. In addition, V_{rd} also plays the role of preventing spontaneous dissociation in the case that XH is a strong acid. The force constant and structural parameters in V_{rd} are appropriately selected (see Table S1 in the Supporting Information for detailed form and parameter values) to keep the dummy proton at its place while not causing much deviation for free energy calculation[26,27].

The vertical deprotonation energy gap $\Delta_{dp}E_{XH}$ defined from the derivative of the mapping potential Eq. (4) with respect to η

$$\Delta_{dp}E_{XH} = \frac{\partial E_\eta}{\partial \eta} = E_{X^-} - E_{XH} \quad (5)$$

$<\Delta_{dp}E_{XH}>_\eta$ is estimated as the time average of vertical deprotonation energy gap over a sufficiently long MD trajectory of the mapping potential energy E_η. Thermodynamic integration of $<\Delta_{dp}E_{XH}>_\eta$ over the coupling parameter η from 0 to 1 yields the deprotonation free energy of reaction (3),

$$\Delta_{dp}A_{XH} = A(\eta=1) - A(\eta=0) = \int_0^1 d\eta \langle \Delta_{dp}E_{XH} \rangle_\eta \quad (6)$$

In practice, a few mapping potentials E_η are sampled with DFTMD at η values usually evenly spaced from 0 to 1, and then numerical integration of Eq. (6) is carried out using the trapezoidal rule or Simpson's rule.

In order to obtain the pK_a for reaction (1), the deprotonation of XH needs to be coupled with the deprotonation of aqueous hydronium H_3O^+(aq), i.e. the deprotonation free energy of XH $\Delta_{dp}A_{XH}$ should be referenced to the deprotonation energy of H_3O^+(aq)[27]. Hence, the acid dissociation energy ΔG_a^o and acidity constant of XH can be expressed as

$$\Delta G_a^o = 2.3 k_B T p K_a = \Delta_{dp}A_{XH} - \Delta_{dp}A_{H_3O^+} + k_B T \ln\left[c^o \Lambda_{H^+}^3\right] \quad (7)$$

in which $\Delta_{dp}A_{H_3O^+}$ is the deprotonation free energy of H_3O^+(aq), and the added constant $k_B T \ln\left[c^o \Lambda_{H^+}^3\right]$ is the translational entropy of proton, accounting for the acid dissociation entropy[27]. $\Delta_{dp}A_{H_3O^+}$ can be calculated using the same thermodynamic integration method described above, and should be evaluated in the same periodic model as the $\Delta_{dp}A_{XH}$ in order to cancel the so-called Hartree potential shift present in both terms due to the uncertainty in potential reference under periodic boundary conditions. We refer interested readers to the previous publications about details on Hartree potential shift[26, 28, 30].

It is expensive to evaluate the reference integral $\Delta_{dp}A_{H_3O^+}$ in large interface models. To save the computational costs, the $\Delta_{dp}A_{H_3O^+}$ term in Eq. (7) can be obtained by combining the integral computed in a pure water box, which is much less costly and already known from the previous work, and a secondary step of aligning electrostatic (Hartree) potentials in bulk water region between the interface model and pure water model[54]. This method has been presented in detail in Ref. 54, and can be simply written as follows:

$$\Delta_{dp}A_{H_3O^+}^{(i)} = \Delta_{dp}A_{H_3O^+}^{(w)} - e\phi_{wat}^{(i)} \quad (8)$$

in which the added superscript '(i)' and '(w)' represent the oxide/water interface and pure water model, respectively, and $\phi_{wat}^{(i)}$ is the average electrostatic potential of the water phase in the oxide/water interface model. $\Delta_{dp}A_{H_3O^+}^{w}$ has been calculated using both 32 and 64 water box and the recommended value is 15.35 eV[28,55]. The $-e\phi_{wat}^{(i)}$ can be obtained by averaging over the DFTMD trajectory using the interface model.

This DFTMD method for pK_a calculation has been extensively applied to aqueous solution and oxide interfaces and carefully analyzed for errors in previous studies, including density functionals, finite size errors and statistical errors[24,26,28]. It has been found that the main error for pK_a calculation comes from statistical uncertainties, which is on the order of ~0.1 eV, i.e. 1-2 pK_a units.

2.2. Calculating pK_a's of proton hopping systems

When calculating the potential energy function E_{X^-} of deprotonated species in which the acid proton was transformed into a dummy proton, the original X⁻ site could accept another proton H_h hopping from neighboring sites, as illustrated in Fig.1 (a). The configuration of such two overlapped or extremely close protons presents numerical challenges, as it will lead to divergence in the electronic structure calculation. Therefore, techniques need to be introduced to prevent X⁻ away from receiving spontaneously transferred protons from neighboring acids.

A simple fix to this problem is applying harmonic restraining potentials V_{rH} to all O-H bonds (see Table S1 in the Supporting Information for detailed form and parameters)[24,26], as illustrated in Fig. 1(b). However, for solid-liquid interfaces where water dissociation is reversible and proton hopping between surface groups is spontaneous, this practice is questionable because it eliminates all PT events in the system.

In this work, we propose to use, instead of V_{rH}, a set of repulsive potentials V_{rep} described in Fig. 1(c). Not only does this prevent X⁻ from receiving protons (while also preventing proton overlap), it also allows PT events to happen in the rest parts of the system, providing a more accurate description of the chemical environment.
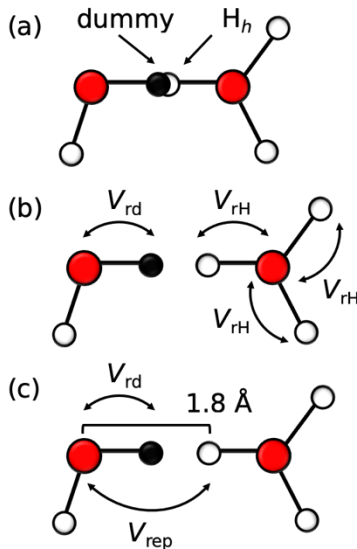
Figure 1. Simplified illustration of the insertion of an acid proton by converting the dummy proton into a real proton (i.e. a water molecule assumes the role of XH, while we associate a hopping proton H_h with a hydronium ion). (a) In the absence of V_{rH} and V_{rep} constraints, the dummy proton (black circle) and H_h have a significant probability of overlapping. (b) In the V_{rH} scheme, restraining potentials are applied to prevent overlap between the dummy proton and H_h. This also prevents possible dissociation of O-H bonds. (c) In the proposed V_{rep} scheme the dummy proton is still restrained to its oxygen atom, but now overlap is prevented by imposing a repulsive potential between the dummy proton and the other hydrogen atoms in the system.

We choose a Buckingham-type repulsive potential for V_{rep}

$$V_{rep} = A \cdot e^{-d/B} \qquad (9)$$

where d is the distance between the deprotonated group X⁻ and neighboring protons, and A and B are parameters having the unit of energy and length, respectively. It is worth noting that similar to V_{rd} included in Eq. (4), V_{rep} enters the expression of the mapping potential as

$$E_\eta = (1-\eta)E_{XH} + \eta E_{X^-} + V_{rd} + V_{rep} \qquad (10)$$

Since both V_{rd} and V_{rep} are independent of the coupling parameter η, they do not contribute to the vertical energy gaps and surface pK_a's directly. Note that they could still affect the computed pK_a's by perturbing the equilibrium structures, which we hope to minimize in our calculation by carefully choosing the parameters in them. Parameter A (1254.7 eV) and B (0.1724 Å) are determined by reproducing the radial distribution function (RDF) of the reference DFTMD simulation consisting of one OH⁻ in 31 water molecules with the harmonic restraining potential V_{rH}. (Fig. 2). It is worth pointing out that the RDFs obtained with restraints are essentially the same as the unbiased one[56,57], indicating the perturbation caused by the restraint on the structure is negligibly small.
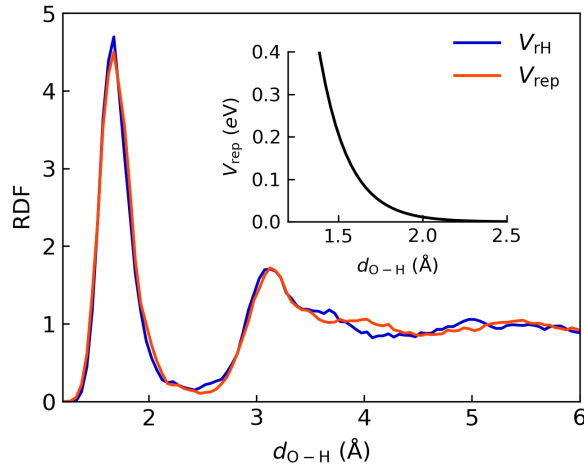

Figure 2. Radial distribution functions (RDF) between O atom of OH⁻ and hydrogen atoms in 31 H_2O cubic box. The blue curve corresponds to the case that all the O-H bonds of water molecules subjected to harmonic restraining potentials V_{rH}, and the orange curve corresponds to the O atom in OH⁻ applied with the Buckingham-type repulsive potentials V_{rep} against the rest H atoms in water. d_{O-H} (Å) is the distance of the O atom in OH⁻ and the H atoms in water. Inset: the variation of V_{rep} changes with d_{O-H} (A=1254.7 eV and B=0.1724 Å).

2.3. Computational setup

We first verify the V_{rep} scheme by calculating the pK_a's of H_2O and aqueous HS⁻ solution, and then apply it to the aqueous $SnO_2(110)/H_2O$ interface. For liquid H_2O and aqueous HS⁻ solution, the simulated models are periodically repeated cubic cells with a width of 9.86 Å consisting of 32 H_2O and 31 H_2O with one HS⁻, respectively.

The $SnO_2(110)$ surface is modelled by periodic slabs of three O-Sn-O layers with lateral dimensions of a 4×2 surface cell. The slabs are separated by a space of 9.7 Å giving an orthorhombic supercell of dimensions $12.7 \times 13.4 \times 19.3$ Å^3. To model the $SnO_2(110)/H_2O$ interface, the space between the slabs is filled with 54 water molecules and there are two symmetric interfacial planes in each unit cell (see Fig. 3).

All the DFTMD calculations are carried out using the freely available program package CP2K/Quickstep[58]. The density functional BLYP[59,60] is used for H_2O and HS$^-$ and the PBE functional[61] is used for $SnO_2(110)/H_2O$ interface. Goedecker-Teter-Hutter (GTH) pseudopotentials[62,63] are employed to represent the core electrons. The atomic basis sets for the valence electrons ($1s^1$ for H, $2s^22p^4$ for O, $3s^23p^4$ for S and $5s^25p^2$ for Sn) are the standard triple-ζ basis with two sets of polarization functions (TZV2P) for H_2O and HS$^-$, and short-ranged double-ζ basis functions with one set of polarization functions (DZVP)[64] for the $SnO_2(110)/H_2O$ interface. The plane wave cutoff for electron density expansion is set as 400 Ry. The target accuracy for the SCF convergence is 3×10^{-7} a.u.. The NVT ensemble is used for MD propagation with the time step of 0.5 fs and the equilibrium temperature for all the simulations is kept to be 330K by using the Nose-Hoover thermostat[65].
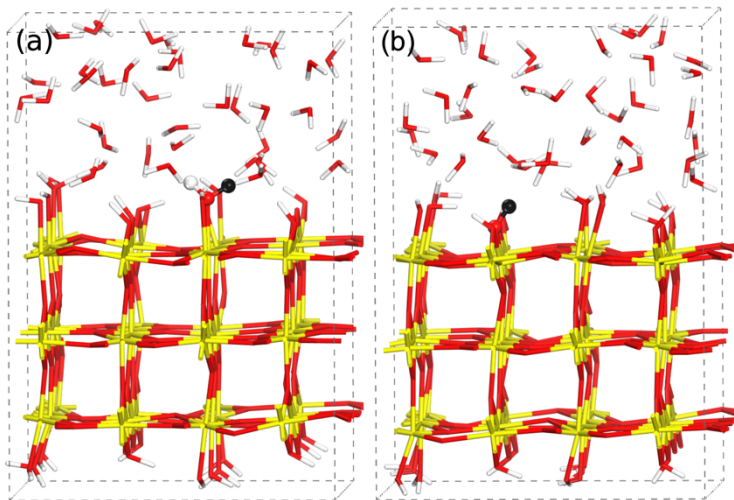
Figure 3. DFTMD models of the $SnO_2(110)/H_2O$ interface used in surface acidity calculation. (a) Model for $Sn_{5c}OH_2/Sn_{5c}OH^-$ site (reaction (11)) and (b) model for $Sn_2O_{br}H^+/Sn_2O_{br}$ site (reaction (12)). Sn, O, H and target proton/dummy are colored in yellow, red, white and black, respectively.

3. Results and discussion

3.1. Validating the V_{rep} scheme by computing pK_a of weak acids H_2O and HS$^-$

According to Eqs. (6) and (7), we calculate the deprotonation integrals ΔA, acid dissociation free energies ΔG_a^o and pK_a's of H_2O and HS$^-$ using the V_{rep} scheme, as listed in Table 1. The previous calculation with the V_{rH} scheme[28], as well as
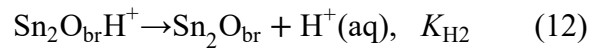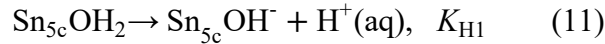
experimental data, are also given for comparison. The computed pK_a's of H_2O and HS⁻ calculated with the V_{rep} scheme are 14.7 and 17.0, respectively, in agreement with the experimental values of 15.7 and 17.0. Furthermore, comparing to the literature values using the V_{rH} scheme, there is also little difference in the computed free energies and pK_a's. These encouraging results indicate that the V_{rep} scheme with properly chosen parameters (see Section 2.2) can indeed give good pK_a's of weak acids.

Table 1. Deprotonation integrals ΔA and conversion to the acid dissociation free energies ΔG_a^o and pK_a's of H_2O and HS⁻, computed with the V_{rH} and V_{rep} scheme in comparison with the experimental values. All the energies are in eV, and the estimated statistical errors for the energies are on the order of ~0.1 eV.

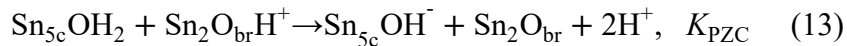| deprotonation	GGA/BLYP (V_{rep})			GGA/BLYP (V_{rH})[28]			Exp.	
	ΔA	ΔG_a^o	pK_a	ΔA	ΔG_a^o	pK_a	ΔG_a^o	pK_a
$H_2O(l) \rightarrow OH^-$	16.37	0.83	14.7	16.34	0.70	13.6	0.83	15.7
$HS^- \rightarrow S^{2-}$	16.54	1.0	17.0	16.5	1.0	17.1	1.0	17.0

3.2. Applying the V_{rep} scheme for computing surface pK_a's of SnO₂ (110)

Cassiterite SnO_2 is isostructural to rutile TiO_2. As in the previous pK_a calculation at the rutile $TiO_2(110)/H_2O$ interface[36], there are two active sites in which may exchange protons with solution, i.e. the terminal five-coordinated Sn_{5c} group and the bridging oxygen O_{br} group. The corresponding half-reactions are

$$Sn_{5c}OH_2 \rightarrow Sn_{5c}OH^- + H^+(aq), \quad K_{H1} \qquad (11)$$

$$Sn_2O_{br}H^+ \rightarrow Sn_2O_{br} + H^+(aq), \quad K_{H2} \qquad (12)$$

where K_{H1} and K_{H2} are the deprotonation equilibrium constants, and the respective pK_a = -log K_H. The solvated proton $H^+(aq)$ is the reference for the pK_a calculation. Reaction (11) describes a scenario in which a water molecule adsorbed on a terminal metal site releases a proton to solution, rendering the surface negatively charged (i.e. pH > PZC). The reverse of reaction (12) indicates a bridging oxygen site receiving a proton from solution, which positively charges the surface (i.e. pH < PZC). The same as the aqueous $TiO_2(110)$ surface[36], the PZC on $SnO_2(110)$ can be achieved by adding reactions (11) and (12), while dissociation of surface terminal water can be described by subtracting reaction (11) from reaction (12)

$$Sn_{5c}OH_2 + Sn_2O_{br}H^+ \rightarrow Sn_{5c}OH^- + Sn_2O_{br} + 2H^+, \quad K_{PZC} \qquad (13)$$

$$Sn_{5c}OH_2 + Sn_2O_{br} \rightarrow Sn_{5c}OH^- + Sn_2O_{br}H^+, \quad K_d \qquad (14)$$

In addition, the ratio of Sn_{5c} sites and Sn_2O_{br} sites on the $SnO_2(110)$ surface is 1:1, and the surface concentrations of $Sn_{5c}OH^-$ and $Sn_2O_{br}H^+$ are equal at the PZC equilibrium, which leads to $K_{PZC} = [H^+]^2_{PZC} = K_{H1}K_{H2}$ and $K_d = K_{H1}/K_{H2}$. Substituting $\Delta A_{diss} = -k_B T \ln K_d$ and $pK_a = -\log K_H$ in the above equations, the relation between pK_a, PZC and the dissociation free energy of surface absorbed water are derived as follows

$$PZC = \frac{1}{2}\left(pK_{a1} + pK_{a2}\right) \qquad (15)$$

$$\Delta A_{diss} = 2.30 k_B T\left(pK_{a1} - pK_{a2}\right) \qquad (16)$$

For the $SnO_2(110)/H_2O$ interface model, the value of $\phi_{wat}^{SnO_2(110)}$ in Eq. (8) is found to be 4.05 V, which leads to a value of $\Delta_{dp}A_{H_3O^+}^{SnO_2(110)}$ of 19.4 eV. The time accumulative averages of vertical energy gaps and computed deprotonation integrals of $\Delta_{dp}A_{Sn_{5c}OH_2}$ and $\Delta_{dp}A_{Sn_2O_{br}H^+}$ are illustrated in Figure S1 in the Supporting Information. Substituting $\Delta_{dp}A_{Sn_{5c}OH_2}$ and $\Delta_{dp}A_{Sn_2O_{br}H^+}$ and aligned $\Delta_{dp}A_{H_3O^+}^{SnO_2(110)}$ into Eq. (7) gives the pK_a's values. The intrinsic pK_a's for $Sn_{5c}OH_2$ (pK_{a1}) and $Sn_2O_{br}H^+$ (pK_{a2}) calculated with the V_{rep} scheme are found to be 4.4 and 4.7, respectively. The computed pK_{a1} and pK_{a2} are close, and their average gives the PZC of 4.6 following Eq. (15). The dissociation free energy ΔA_{diss} of terminal water is -0.02 eV according to Eq. (16). All the calculated results are listed in Table 2.

In terms of experimental values, Bogdanova et al[66] found a PZC of 4.1 at 20°C from potentiometric titrations with nanosized SnO_2, and Rosenqvist et al[67] obtained a similar PZC value of ~4.3 at 25°C for tin oxide power using the same titration method. In an earlier work, Ahmed and Maksimov[68] determined the PZC for crystalline cassiterite to be in the range 4.8 - 5.5. It is clear that the DFTMD calculation with the V_{rep} scheme gives the PZC value of 4.6, almost the same as experiment.

In contrast, the intrinsic pK_a's for $Sn_{5c}OH_2$ (pK_{a1}) and $Sn_2O_{br}H^+$ (pK_{a2}) calculated with the V_{rH} scheme are 5.6 and -0.1, respectively. The statistical convergence of vertical energy gaps and deprotonation integrals of $\Delta_{dp}A_{Sn_{5c}OH_2}$ and $\Delta_{dp}A_{Sn_2O_{br}H^+}$ is shown in Figure S2 in the Supporting Information. Thus, the computed PZC is 2.8 following Eq. (15) and the dissociation free energy ΔA_{diss} of surface water is 0.34 eV according to Eq. (16). Comparing to the V_{rep} scheme (see Table 2), the V_{rH} scheme underestimates the PZC and significantly overestimates ΔA_{diss}.

Table 2. Comparison between computed pK_a's for $Sn_{5c}OH_2$ (pK_{a1}) and $Sn_2O_{br}H^+$ (pK_{a2}), PZC, ΔpK_a and dissociation free energy ΔA_{diss} of surface water using the V_{rep} and V_{rH} scheme.

pK_{a1}	pK_{a2}	PZC	ΔpK_a	ΔA_{diss} /eV

V_{rep} scheme	4.4	4.7	4.6	-0.3	-0.02
V_{rH} scheme	5.6	-0.1	2.8	5.7	0.34

3.3 Interpreting the effect of repulsive potential V_{rep} on pK_a shifts

When comparing pK_a shifts due to the V_{rH} scheme and the V_{rep} scheme, the most significant change happens to pK_{a2} (Eq. 12 and Table 2). Here we investigate possible causes of the observed differences.

At face value, the main difference between the V_{rH} scheme and the V_{rep} scheme is that the latter allows PT events happen in the neighboring surface groups. This could lead to the stabilization of charged groups ($Sn_2O_{br}H^+$ and $Sn_{5c}OH^-$) due to the dissociated water nearby and a possible charge equilibration mechanism. As a consequence, we would expect pK_{a2} to increase and pK_{a1} to decrease to the similar extent when changing from the V_{rH} to V_{rep} scheme. However, this is clearly not the case, as evidenced by Table 2. Despite the correct signs, pK_a shifts are asymmetric and significantly larger in the case of pK_{a2}. This suggests that there is a second factor resulting from the V_{rep} scheme which also affects pK_a shifts.

By analyzing the structures of surface groups involved in the deprotonation reactions in Eq. 11 and Eq. 12, we find that the V_{rep} scheme promotes H-bonds forming between $Sn_{5c}OH_2$ and neighboring $Sn_{5c}OH^-$ in the simulation of the $Sn_{5c}OH_2$ protonation state (Fig. 4f), and also between $Sn_2O_{br}H^+$ and $Sn_{5c}OH^-$ in the simulation of the $Sn_2O_{br}H^+$ protonation state (Fig. 5f). When comparing to the result using the V_{rH} scheme (Fig. 4a and Fig. 5a), this effect is more significant between $Sn_2O_{br}H^+$ and $Sn_{5c}OH^-$, as shown in the RDFs and coordination numbers (Fig. 4b and Fig. 5b).

Forming H-bonds with neighboring surface groups will stabilize $Sn_2O_{br}H^+$ and $Sn_{5c}OH_2$. Consequently, both pK_{a2} and pK_{a1} should become larger. Thus, when this hydrogen bonding effect acts to further enhance the differences in pK_{a2} between the V_{rH} and V_{rep} scheme, it competes with the charge stabilization mechanism discussed above when considering pK_{a1}. The fact that pK_{a1} changes by only a little suggests that the effect of hydrogen bonding is in fact rather significant.
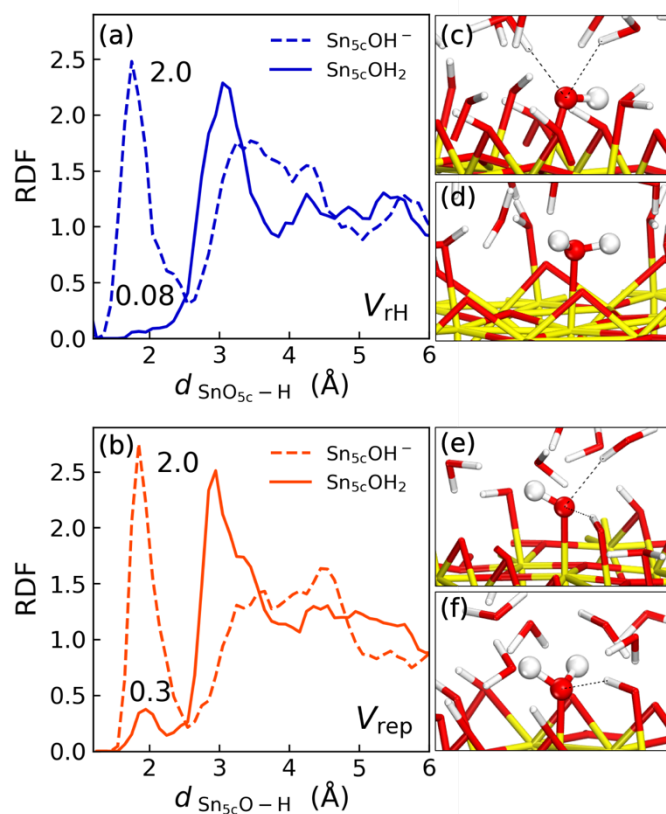
Figure 4. Structural analysis of surface groups involved in pK_{a1} calculations (reaction (11)). (a) The RDFs between surface groups and neighboring protons using the V_{rH} scheme. (b) The RDFs between surface groups and neighboring protons using the V_{rep} scheme. Numbers next to the first peak of the RDFs are the coordination numbers. The corresponding DFTMD snapshots of $Sn_{5c}OH^-$ and $Sn_{5c}OH_2$ are shown in (c) and (d) for V_{rH} and (e) and (f) for V_{rep}.
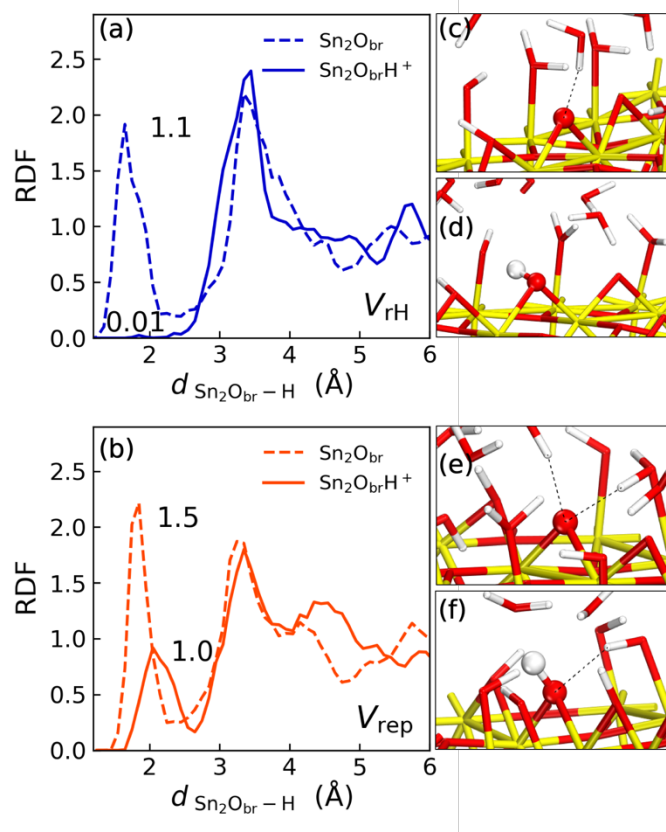
Figure 5. Structural analysis of surface groups involved in pK_{a2} calculations (reaction (12)). (a) The RDFs between surface groups and neighboring protons using the V_{rH} scheme. (b) The RDFs between surface groups and neighboring protons using the V_{rep} scheme. Numbers next to the first peak of the RDFs are the coordination numbers. The corresponding DFTMD snapshots of Sn_2O_{br} and $Sn_2O_{br}H^+$ are shown in (c) and (d) for V_{rH} and (e) and (f) for V_{rep}.

The remaining question is why the V_{rep} scheme promotes H-bonds forming between surface groups while the V_{rH} scheme does not. As shown in Fig. 6, one can clearly see that when a H-bond is formed between the adsorbed water and the bridge oxygen in the case of the V_{rep} scheme, the O-H bond length is significantly larger than what is allowed by the V_{rH} scheme. In other words, the difference between two schemes not only lies in the availability of PT events but also shows up in the H-bond network at solid-liquid interfaces.
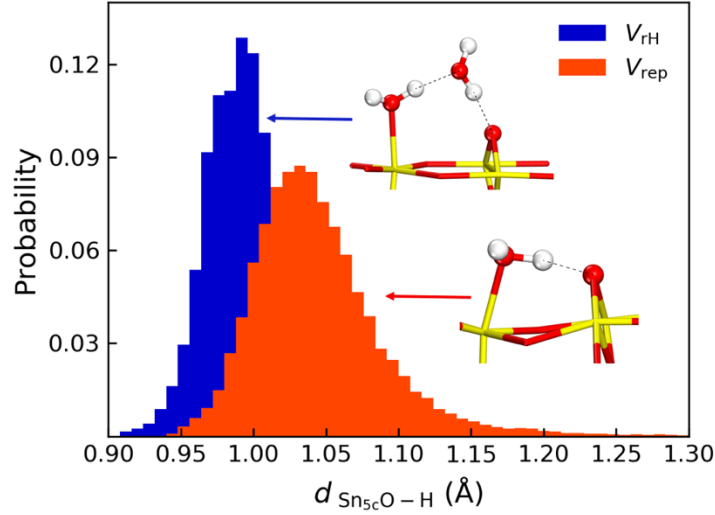
Figure 6. Distribution of O-H distance in the adsorbed water molecules (i.e. $Sn_{5c}OH_2$ groups) that forms direct H-bonds, with surface bridging oxygens (i.e. Sn_2O_{br} groups) when using the V_{rep} scheme, and with a water molecule when using the V_{rH} scheme.

3.4 Acidities of surface groups at acid-base equilibrium

Assuming that dissociation events are independent, the degree of dissociation α is linked to ΔA_{diss},

$$K_d = \exp\left(-\frac{\Delta A_{diss}}{k_B T}\right) = \frac{\alpha^2}{(1-\alpha)^2} \qquad (17)$$

ΔA_{diss} can therefore be estimated by simply counting the degree of dissociation in an unbiased DFTMD trajectory. We set the O-H bond length cutoff as 1.25 Å. Averaging over a 15 ps DFTMD trajectory, we obtain the number of surface sites $Sn_2O_{br}H^+$ and Sn_2O_{br} being 4.53 and 3.47 in our $SnO_2(110)$/water interface model (8 sites in total on the surface), respectively. Thus, the degree of dissociation α is estimated as 57% at the $SnO_2(110)/H_2O$ interface. This corresponds to almost zero ΔA_{diss}, which indeed agrees with the value of -0.02 eV calculated from ΔpK_a with the V_{rep} scheme.

Finally, we would like to link our calculation of similar pK_a's of the two sites on SnO_2 with the general consideration of thermodynamics of acid-base equilibrium at oxide-water interfaces. For oxide surfaces with frequent proton hopping, acid-base equilibrium can be readily established at the time scale of our simulation. As a result, the calculated deprotonation free energies of the two sites would be necessarily the same, leading to both pK_a's being the same as PZC. In a strict sense, the pK_a is defined for acid dissociation taking at the dilute limit, and thus ignoring the

interaction among the conjugate acid and base. However, on SnO_2 such a condition is not valid since partial water dissociation with frequent proton hopping has already implied strong mutual interaction in the mixture of two pairs of acid/base conjugate sites.

4. Summary and outlook

In summary, we extend the methodology of combining DFTMD and free energy perturbation for computing surface pK_a's to systems involving weak acids and spontaneous proton hopping. The key idea is to use a repulsive potential V_{rep} between the deprotonated group X^- and all surrounding protons in the pK_a calculations, instead of applying harmonic restraints V_{rH} to all O-H bonds.

In the case of $SnO_2(110)/H_2O$ interface where water dissociation is reversible and proton hopping is spontaneous, we showed that only the V_{rep} scheme leads to good agreement with experiment in terms of the PZC and with the unbiased DFTMD simulation for the degree of water dissociation.

Furthermore, it is found that the V_{rep} scheme not only allows PT events happen in the simulation system but also promotes H-bonds formation between surface groups, comparing to the V_{rH} scheme. This explains the extend of pK_a shifts when switching from the V_{rH} scheme to the V_{rep} scheme and provides a more realistic description of the corresponding solid-liquid interface. Our calculation gives two similar pK_a's for the two surface sites, indicating that water dissociation free energy at the proton hopping interface is close to zero, as expected from the acid-base equilibrium.

Since the V_{rep} scheme is validated in this work and generally applicable to systems involving weak acids and spontaneous proton hopping, we expect that it would be useful to other solid-liquid interfaces commonly found in electrochemistry, geochemistry and environmental science.

Supporting Information Available

Description of the harmonic restraining potentials used in the method for computing deprotonation free energies, as well as calculation of vertical energy gaps and deprotonation integrals, are given in the Supporting Information. This information is available free of charge via the Internet at http://pubs.acs.org/.

References

(1) Tuladhar, A.; Piontek, S. M.; Borguet, E. Insights on Interfacial Structure, Dynamics, and Proton Transfer from Ultrafast Vibrational Sum Frequency Generation Spectroscopy of the Alumina(0001)/Water Interface. *J. Phys. Chem. C.* **2017**, *121*, 5168-5177.

(2) Kisch, H. Semiconductor Photocatalysis for Chemoselective Radical Coupling Reactions. *Accounts Chem. Res.* **2017**, *50*, 1002-1010.

(3) Sulpizi, M.; Gaigeot, M. P.; Sprik, M. The Silica-Water Interface: How the Silanols Determine the Surface Acidity and Modulate the Water Properties. *J. Chem. Theory Comput.* **2012**, *8*, 1037-1047.

(4) Gaigeot, M. P.; Sprik, M.; Sulpizi, M. Oxide/water interfaces: how the surface chemistry modifies interfacial water properties. *J. Phys.: Condens. Matter.* **2012**, *24*, 11.

(5) Tazi, S.; Rotenberg, B.; Salanne, M.; Sprik, M.; Sulpizi, M. Absolute acidity of clay edge sites from ab-initio simulations. *Geochim. Cosmochim. Acta.* **2012**, *94*, 1-11.

(6) Leung, K.; Criscenti, L. J. Predicting the acidity constant of a goethite hydroxyl group from first principles. *J. Phys.: Condens. Matter.* **2012**, *24*, 9.

(7) De Meyer, T.; Ensing, B.; Rogge, S. M. J.; De Clerck, K.; Meijer, E. J.; Van Speybroeck, V. Acidity Constant (pK(a)) Calculation of Large Solvated Dye Molecules: Evaluation of Two Advanced Molecular Dynamics Methods. *Chemphyschem.* **2016**, *17*, 3447-3459.

(8) Kilic, M.; Ensing, B. Acidity constants of lumiflavin from first principles molecular dynamics simulations. *Phys. Chem. Chem. Phys.* **2014**, *16*, 18993-19000.

(9) Pfeiffer-Laplaud, M.; Gaigeot, M. P.; Sulpizi, M. pK(a) at Quartz/Electrolyte Interfaces. *J. Phys. Chem. Lett.* **2016**, *7*, 3229-3234.

(10) Stumm, W., *Chemistry of the solid-water interface: processes at the mineral-water and particle-water interface in natural systems*; John Wiley & Son Inc.: New York, USA, **1993**.

(11) Bickmore, B. R.; Rosso, K. M.; Tadanier, C. J.; Bylaska, E. J.; Doud, D. Bond-valence methods for pK(a) prediction. II. Bond-valence, electrostatic, molecular geometry, and solvation effects. *Geochim. Cosmochim. Acta*. **2006**, *70*, 4057-4071.

(12) Ardizzone, S.; Trasatti, S. Interfacial properties of oxides with technological impact in electrochemistry. *Adv. Colloid Interface Sci.* **1996**, *64*, 173-251.

(13) McBriarty, M. E.; von Rudorff, G. F.; Stubbs, J. E.; Eng, P. J.; Blumberger, J.; Rosso, K. M. Dynamic Stabilization of Metal Oxide-Water Interfaces. *J. Am. Chem. Soc.* **2017**, *139*, 2581-2584.

(14) Macias-Romero, C.; Nahalka, I.; Okur, H. I.; Roke, S. Optical imaging of surface chemistry and dynamics in confinement. *Science* **2017**, *357*, 784-787.

(15) Sung, J.; Shen, Y. R.; Waychunas, G. A. The interfacial structure of water/protonated α-Al$_2$O$_3$(11$\bar{2}$0) as a function of pH. *J. Phys.: Condens. Matter.* **2012**, *24*, 124101.

(16) Catalano, J. G.; Park, C.; Fenter, P.; Zhang, Z. Simultaneous inner- and outer-sphere arsenate adsorption on corundum and hematite. *Geochimica et Cosmochimica Acta.* **2008**, *72*, 1986-2004.

(17) Bickmore, B. R.; Tadanier, C. J.; Rosso, K. M.; Monn, W. D.; Eggett, D. L. Bond-Valence methods for pK(a) prediction: critical reanalysis and a new approach. *Geochim. Cosmochim. Acta.* **2004**, *68*, 2025-2042.

(18) Bond Valences. In *Bond Valences*; Brown, I. D., Poeppelmeier, K. R., Eds.; Structure and Bonding; Springer-Verlag Berlin: Berlin, **2014**; *158*, 1-262.

(19) Bickmore, B. R.; Rosso, K. M.; Brown, I. D.; Kerisit, S. Bond-Valence Constraints on Liquid Water Structure. *J. Phys. Chem. A* **2009**, *113*, 1847-1857.

(20) Hiemstra, T.; Venema, P.; VanRiemsdijk, W. H. Intrinsic proton affinity of reactive surface groups of metal (hydr)oxides: The bond valence principle. *J. Colloid Interface Sci.* **1996**, *184*, 680-692.

(21) Machesky, M. L.; Predota, M.; Wesolowski, D. J.; Vlcek, L.; Cummings, P. T.; Rosenqvist, J.; Ridley, M. K.; Kubicki, J. D.; Bandura, A. V.; Kumar, N.; Sofo, J. O. Surface Protonation at the Rutile (110) Interface: Explicit Incorporation of Solvation Structure within the Refined MUSIC Model Framework. *Langmuir* **2008**, *24*, 12331-12339.

(22) Vlcek, L.; Zhang, Z.; Machesky, M. L.; Fenter, P.; Rosenqvist, J.; Wesolowski, D. J.; Anovitz, L. M.; Predota, M.; Cummings, P. T. Electric double layer at metal oxide surfaces: Static properties of the cassiterite - Water interface. *Langmuir* **2007**, *23*, 4925-4937.

(23) Rosenqvist, J.; Machesky, M. L.; Vlcek, L.; Cummings, P. T.; Wesolowski, D. J. Charging Properties of Cassiterite (alpha-SnO_2) Surfaces in NaCl and RbCl Ionic Media. *Langmuir* **2009**, *25*, 10852-10861.

(24) Sulpizi, M.; Sprik, M. Acidity constants from vertical energy gaps: density functional theory based molecular dynamics implementation. *Phys. Chem. Chem. Phys.* **2008**, *10*, 5238-5249.

(25) Sulpizi, M.; Sprik, M. Acidity constants from DFT-based molecular dynamics simulations. *J. Phys.: Condens. Matter.* **2010**, *22*, 284116.

(26) Cheng, J.; Sulpizi, M.; Sprik, M. Redox potentials and pK_a for benzoquinone from density functional theory based molecular dynamics. *J. Chem. Phys.* **2009**, *131*, 154504.

(27) Costanzo, F.; Sulpizi, M.; Della Valle, R. G.; Sprik, M. The oxidation of tyrosine and tryptophan studied by a molecular dynamics normal hydrogen electrode. *J. Chem. Phys.* **2011**, *134*, 21.

(28) Cheng, J.; Liu, X.; VandeVondele, J.; Sulpizi, M.; Sprik, M. Redox potentials and acidity constants from density functional theory based molecular dynamics. *Acc. Chem. Res.* **2014**, *47*, 3522-3529.

(29) Cheng, J.; Liu, X.; Kattirtzi, J. A.; VandeVondele, J.; Sprik, M. Aligning electronic and protonic energy levels of proton-coupled electron transfer in water oxidation on aqueous TiO_2. *Angew. Chem., Int. Ed.* **2014**, *53*, 12046-12050.

(30) Cheng, J.; Sprik, M.: Alignment of electronic energy levels at electrochemical interfaces. *Phys. Chem. Chem. Phys.* **2012**, *14*, 11245-11267.

(31) Liu, X. D.; Cheng, J.; Sprik, M.; Lu, X. C.; Wang, R. C. Interfacial structures and acidity of edge surfaces of ferruginous smectites. *Geochim. Cosmochim. Acta.* **2015**, *168*, 293-301.

(32) Liu, X. D.; Lu, X. C.; Sprik, M.; Cheng, J.; Meijer, E. J.; Wang, R. C. Acidity of edge surface sites of montmorillonite and kaolinite. *Geochim. Cosmochim. Acta.* **2013**, *117*, 180-190.

(33) Liu, X. D.; He, M. J.; Lu, X. C.; Wang, R. C. Structures and acidity constants of arsenite and

thioarsenite species in hydrothermal solutions. *Chem. Geol.* **2015**, *411*, 192-199.

(34) Liu, X. D.; Cheng, J.; Lu, X. C.; Wang, R. C. Surface acidity of quartz: understanding the crystallographic control. *Phys. Chem. Chem. Phys.* **2014**, *16*, 26909-26916.

(35) Liu, X. D.; Cheng, J.; He, M. J.; Lu, X. C.; Wang, R. C. Acidity constants and redox potentials of uranyl ions in hydrothermal solutions. *Phys. Chem. Chem. Phys.* **2016**, *18*, 26040-26048.

(36) Cheng, J.; Sprik, M. Acidity of the Aqueous Rutile TiO_2(110) Surface from Density Functional Theory Based Molecular Dynamics. *J. Chem. Theory Comput.* **2010**, *6*, 880-889.

(37) Cheng, J.; Liu, X.; VandeVondele, J.; Sprik, M. Reductive Hydrogenation of the Aqueous Rutile TiO_2(110) Surface. *Electrochim. Acta.* **2015**, *179*, 658-667.

(38) Gittus, O. R.; von Rudorff, G. F.; Rosso, K. M.; Blumberger, J. Acidity Constants of the Hematite-Liquid Water Interface from Ab Initio Molecular Dynamics. *J. Phys. Chem. Lett.* **2018**, *9*, 5574-5582.

(39) Blumberger, J.; Tavernelli, I.; Klein, M. L.; Sprik, M. Diabatic free energy curves and coordination fluctuations for the aqueous Ag^+/Ag^{2+} redox couple: A biased Born-Oppenheimer molecular dynamics investigation. *J. Chem. Phys.* **2006**, *124*, 12.

(40) King, G.; Warshel, A. Investigation of the free-energy functions for electron-transfer reactions. *J. Chem. Phys.* **1990**, *93*, 8682-8692.

(41) Lee, F. S.; Chu, Z. T.; Bolger, M. B.; Warshel, A. Calculations of antibody antigen interactions-microscopic and semimicroscopic evaluation of the free-energies of binding of phosphorylcholine analogs to MCPC603. *Protein Eng.* **1992**, *5*, 215-228.

(42) Kundu, S.; Vidal, A. B.; Yang, F.; Ramírez, P. J.; Senanayake, S. D.; Stacchiola, D.; Evans, J.; Liu, P.; Rodriguez, J. A. Special Chemical Properties of RuOxNanowires in RuO_x/TiO_2(110): Dissociation of Water and Hydrogen Production. *J. Phys. Chem. C* **2012**, *116*, 4767-4773.

(43) Siahrostami, S.; Vojvodic, A. Influence of Adsorbed Water on the Oxygen Evolution Reaction on Oxides. *J. Phys. Chem. C.* **2015**, *119*, 1032-1037.

(44) Tocci, G.; Michaelides, A. Solvent-Induced Proton Hopping at a Water-Oxide Interface. *J. Phys. Chem. Lett.* **2014**, *5*, 474-480.

(45) Quaranta, V.; Hellstrom, M.; Behler, J. Proton-Transfer Mechanisms at the Water-ZnO Interface: The Role of Presolvation. *J. Phys. Chem. Lett.* **2017**, *8*, 1476-1483.

(46) Sato, R.; Ohkuma, S.; Shibuta, Y.; Shimojo, F.; Yamaguchi, S. Proton Migration on Hydrated Surface of Cubic ZrO_2:Ab initioMolecular Dynamics Simulation. *J. Phys. Chem. C* **2015**, *119*, 28925-28933.

(47) Wood, B. C.; Schwegler, E.; Choi, W. I.; Ogitsu, T. Hydrogen-Bond Dynamics of Water at the Interface with InP/GaP(001) and the Implications for Photoelectrochemistry. *J. Am. Chem. Soc.* **2013**, *135*, 15774-15783.

(48) Iyer, A.; Del-Pilar, J.; King'ondu, C. K.; Kissel, E.; Garces, H. F.; Huang, H.; El-Sawy, A. M.; Dutta, P. K.; Suib, S. L. Water Oxidation Catalysis using Amorphous Manganese Oxides, Octahedral Molecular Sieves (OMS-2), and Octahedral Layered (OL-1) Manganese Oxide Structures. *J. Phys. Chem. C* **2012**, *116*, 6474-6483.

(49) Wang, H. W.; Wesolowski, D. J.; Proffen, T. E.; Vlcek, L.; Wang, W.; Allard, L. F.; Kolesnikov, A. I.; Feygenson, M.; Anovitz, L. M.; Paul, R. L. Structure and Stability of SnO_2 Nanocrystals and Surface-Bound Water Species. *J. Am. Chem. Soc.* **2013**, *135*, 6885-6895.

(50) Bandura, A.; Sofo, J.; Kubicki, J. Derivation of Force Field Parameters for SnO_2-H_2O

Surface Systems from Plane-Wave Density Functional Theory Calculations. *J. Phys. Chem. B* **2006**, *110*, 8386-8397.

(51) Yue, J.; Jiang, X.; Yu, A. Adsorption of the OH Group on SnO$_2$(110) Oxygen Bridges: A Molecular Dynamics and Density Functional Theory Study. *J. Phys. Chem. C* **2013**, *117*, 9962-9969.

(52) Bezzerrouk, M. A.; Hassan, M.; Baghdad, R.; Reguieg, S.; Bousmaha, M.; Kharroubi, B.; Bouhafs, B. Thermodynamic, structural and electronic, properties of SnO2: By GGA and GGA + trans-blaha-modified Becke–Johnson (TB-mBJ) calculation. *Superlattices Microstruct.* **2015**, *84*, 80-90.

(53) Sprik, M. Computation of the pK of liquid water using coordination constraints. *Chem. Phys.* **2000**, *258*, 139-150.

(54) Le, J. B.; Iannuzzi, M.; Cuesta, A.; Cheng, J. Determining Potentials of Zero Charge of Metal Electrodes versus the Standard Hydrogen Electrode from Density-Functional-Theory-Based Molecular Dynamics. *Phys. Rev. Lett.* **2017**, *119*, 6.

(55) Cheng, J.; VandeVondele, J. Calculation of Electrochemical Energy Levels in Water Using the Random Phase Approximation and a Double Hybrid Functional. *Phys. Rev. Lett.* **2016**, *116*, 5.

(56) Tuckerman, M.; Laasonen, K.; Sprik, M.; Parrinello, M. Ab initio molecular dynamics simulation of the solvation and transport of hydronium and hydroxyl ions in water. *J. Chem. Phys.* **1995**, *103*, 150-161.

(57) Zhang, W.; van Duin, A. C. T. Second-Generation ReaxFF Water Force Field: Improvements in the Description of Water Density and OH-Anion Diffusion. *J. Phys. Chem. B* **2017**, *121*, 6021-6032.

(58) The CP2K developers group. http://cp2k.berlios.de, 2010.

(59) Becke, A. D. Density-functional exchange-energy approximation with correct asymptotic behavior. *Phys. Rev. A* **1988**, *38*, 3098-3100.

(60) Lee, C. T.; Yang, W. T.; Parr, R. G. Development of the colle-salvetti corralation-energy formula into a functional of the electron-density. *Phys. Rev. B* **1988**, *37*, 785-789.

(61) Perdew, J. P.; Burke, K.; Ernzerhof, M. Generalized gradient approximation made simple. *Phys. Rev. Lett.* **1996**, *77*, 3865-3868.

(62) Goedecker, S.; Teter, M.; Hutter, J. Separable dual-space Gaussian pseudopotentials. *Phys. Rev. B* **1996**, *54*, 1703-1710.

(63) Hartwigsen, C.; Goedecker, S.; Hutter, J. Relativistic separable dual-space Gaussian pseudopotentials from H to Rn. *Phys. Rev. B* **1998**, *58*, 3641-3662.

(64) VandeVondele, J.; Hutter, J. Gaussian basis sets for accurate calculations on molecular systems in gas and condensed phases. *J. Chem. Phys.* **2007**, *127*.

(65) VandeVondele, J.; Mohamed, F.; Krack, M.; Hutter, J.; Sprik, M.; Parrinello, M. The influence of temperature and density functional models in ab initio molecular dynamics simulation of liquid water. *J. Chem. Phys.* **2005**, *122*, 6.

(66) Bogdanova, N. F.; Klebanov, A. V.; Ermakova, L. E.; Sidorova, M. P.; Aleksandrov, D. A. Adsorption of ions on the surface of tin dioxide and its electrokinetic characteristics in 1 : 1 electrolyte solutions. *Colloid J.* **2004**, *66*, 409-417.

(67) Rosenqvist, J.; Machesky, M. L.; Vlcek, L.; Cummings, P. T.; Wesolowski, D. J. Charging Properties of Cassiterite (α-SnO$_2$) Surfaces in NaCl and RbCl Ionic Media. *Langmuir* **2009**, *25*, 10852-10862.

(68) Ahmed, S. M.; Maksimov, D. Studies of the double layer on cassiterite and rutile. *J. Colloid Interface Sci.* **1969**, *29*, 97-104.

TOC